

Article

# Experimental Study on the Thermal Conductivity of Compacted SPV200 Bentonite

Guo-Liang Ren, Chih-Chung Chung , Chia-En Tsai, Che-Jui Cuo and Wei-Hsing Huang \* 

Department of Civil Engineering, National Central University, Zhongli District, Taoyuan City 320317, Taiwan; 107382605@ncu.edu.tw (G.-L.R.); ccchung@ncu.edu.tw (C.-C.C.); 103322052@ncu.edu.tw (C.-E.T.); 107322054@ncu.edu.tw (C.-J.C.)

\* Correspondence: t321655@ncu.edu.tw; Tel.: +886-3-425-7062

**Abstract:** This study employed two thermal conductivity measuring techniques, including the needle probe-based transient needle-probe method in accordance with ASTM 5334-14 and the surface probe-based transient plane source method in compliance with ISO 22007-2:2015, to examine the thermal conductivity of compacted SPV200 bentonite. The effects of temperature, water content, and dry density on the thermal behavior of SPV200 bentonite were extensively investigated. The test results indicate: (1) thermal conductivity measured by the two methods agreed well, while the transient plane source method exhibited good efficiency; (2) the thermal conductivity of compacted SPV200 increases with water content, dry density, and temperature; (3) three-dimensional representations of the thermal conductivity of SPV200 bentonite as functions of dry density, water content, and temperature were generated to illustrate a clear relationship among them; (4) two multi-parameter models for predicting thermal conductivity of compacted SPV200 bentonite were proposed, and both showed good fits to the experimental data. The results provide a practical approach to the prediction of thermal properties of compacted bentonite, which can be helpful in the coupled thermo-hydro-mechanical analysis of buffer materials.

**Keywords:** thermal conductivity; SPV200; needle probe method; transient plane source method



**Citation:** Ren, G.-L.; Chung, C.-C.; Tsai, C.-E.; Cuo, C.-J.; Huang, W.-H. Experimental Study on the Thermal Conductivity of Compacted SPV200 Bentonite. *Minerals* **2022**, *12*, 932. <https://doi.org/10.3390/min12080932>

Academic Editor: Gianvito Scaringi

Received: 26 June 2022

Accepted: 19 July 2022

Published: 24 July 2022

**Publisher's Note:** MDPI stays neutral with regard to jurisdictional claims in published maps and institutional affiliations.



**Copyright:** © 2022 by the authors. Licensee MDPI, Basel, Switzerland. This article is an open access article distributed under the terms and conditions of the Creative Commons Attribution (CC BY) license (<https://creativecommons.org/licenses/by/4.0/>).

## 1. Introduction

Geological disposal facilities have been widely accepted as a feasible way for final disposal of high-level radioactive waste (HLW) by many nuclear power-generating countries in the world [1–8]. The geological structure of HLW disposal is composed of natural barriers mainly provided by the repository host rock and engineered barriers, consisting of components, such as waste canisters, buffer/backfill, seals, and plugs. The buffer material, commonly made using bentonite, plays a crucial role in the conduction and dissipation of radioactive waste decay heat for the safety and stability of geological repositories. Over the past decades, much research have explored the thermal properties of various types of bentonite. Related experiments can be found in the works of Madsen (1998) and Dixon (2019) on MX80 bentonite [9,10], suggesting that thermal properties can be affected by material source, texture, and dry density, Villar (2000) and Rutqvist (2020) on Febex bentonite, proposing that the thermal conductivity is linearly dependent on saturation in the numerical model [11,12], Ould-Lahoucine et al. (2002) and Huang (2020) on Kunigel-V1 bentonite [13,14], which does not behave very differently from MX80 in terms of the moisture distribution and heat transfer characteristics with the same boundary conditions assumed in the simulation model, Chen and Huang (2004) on ZH-clay which is found to be a temperature-sensitive Ca-bentonite produced in Taiwan [15], Ye et al. (2010) and Xu et al. (2021) on GMZ bentonite, drawing the conclusions that thermal conductivity increased with increasing temperature, and the different pore-size distribution can influence the conductive heat transfer [16,17], and Cho et al. (2008) and Yoon (2019) on Kyeongju bentonite, describing the thermal conductivity of compacted bentonite as a function of water fraction

at each dry density [18,19]. Additionally, there are research indicating that soil thermal conductivity is strongly affected by soil structure and chemical composition [20,21]. All these studies have shown that the thermal conductivity of bentonite is closely related to temperature, dry density, the water content of bentonite, and chemical factors. However, these previous studies on the measurement of thermal conductivity were mostly performed with a needle probe in accordance with ASTM 5334 based on the transient heating method. Meanwhile, a tiny hole with a constant diameter must be drilled carefully through the specimen with the grease-coated needle probe, and related calibration is a demanding process. In addition, the thermal properties of SPV200 bentonite were barely discussed though it originated from the same place as MX80.

Moreover, models have been proposed to predict the thermal conductivity of bentonite. Johansen (1975) proposed a model with four parameters, the degree of saturation, soil bulk density, soil porosity, and mineral composition [22]. Cho (2011) considered the thermal conductivity of the compacted bentonite as a weighted sum of the thermal conductivity of the components [23]. A modified geometric mean model was suggested by Chen (2018) based on multi-parameters (e.g., saturation, dry density, particle density) to predict the thermal conductivity of GO-GMZ bentonite [24]. Machine-learning methods were used by Bang (2020) to predict a thermal conductivity model, while the results of the Gaussian process regression with exponential kernel and the ensemble show the best results [25]. A multiple regression analysis was performed by Yoon (2021) to propose a thermal conductivity model introducing the Kriging model for suitable approximation of highly nonlinear functions [26]. Despite all these fruitful results, the relationship between different parameters of predicting models were seldom displayed in visualization, and models with easily accessible parameters still need to be established for quick prediction.

To seek a non-destructive and efficient approach for the measurement of thermal conductivity, this study aims to provide a systematic approach in the measurement of the thermal conductivity of SPV200 bentonite by both traditional and alternating methods in comparison. Therefore, two thermal-conductivity-measuring techniques, the thermal needle probe traditionally based on the transient needle-probe (NP) method and the surface probe based on the transient plane source (TPS) method [27], were adopted to determine the thermal conductivity of compacted bentonites under varying water contents, dry densities, and temperatures. Furthermore, three-dimensional representations of their relationship were illustrated, and calculation models were proposed in predicting the thermal conductivity of a compacted bentonite.

## 2. Materials and Methods

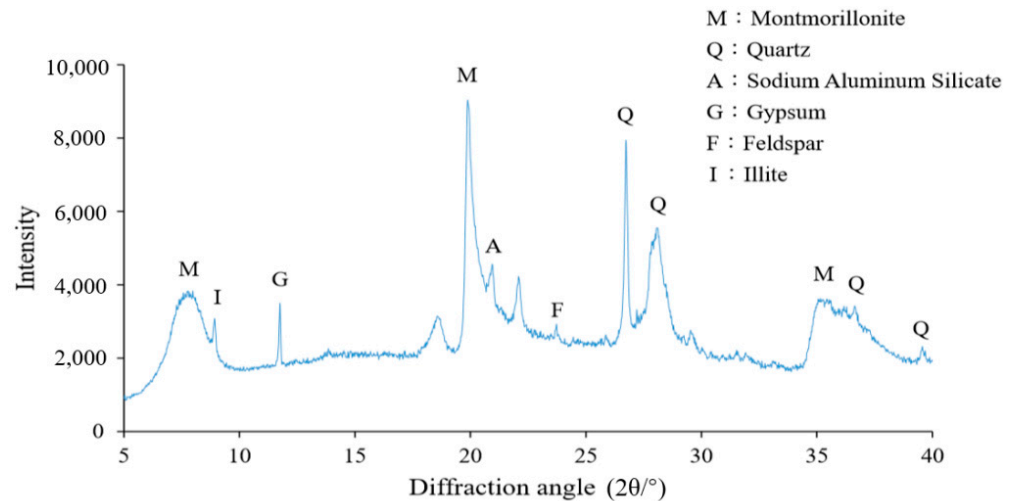
### 2.1. Specimen Preparation

The bentonite used in this study, SPV200 bentonite, is produced by American Colloid Co. Ltd. and originated from the same source as MX-80 but is milled to a fine powder. For many years, it has been a multi-purpose agent used in industrial products where a dry 200-mesh particle size is required. As a selectively mined and processed high-quality sodium bentonite, it is considered a candidate for buffer/backfill material for HLW disposal. The basic physical properties and chemical composition of SPV200 are shown in Table 1.

**Table 1.** Basic properties and chemical composition of SPV200 bentonite.

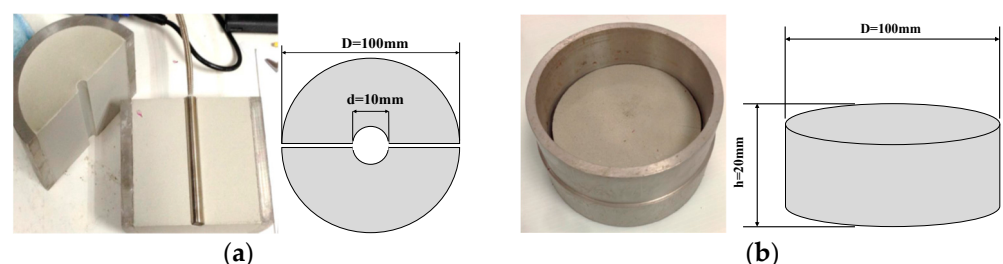
Basic Properties								
Water Content w (%)	Specific Gravity Gs		Liquid Limit LL(%)	Plastic Limit PL(%)		Plastic Index PI		
10.8	2.67		421	43		378		
Chemical Composition (%)								
SiO <sub>2</sub>	Fe <sub>2</sub> O <sub>3</sub>	MgO	CaO	Al <sub>2</sub> O <sub>3</sub>	FeO	Na <sub>2</sub> O	Trace	LOI
63.02	3.25	2.67	0.65	21.08	0.35	2.57	0.72	5.64

Figure 1 shows the X-ray diffraction pattern of SPV200 bentonite. The major minerals identified are montmorillonite and quartz with some sodium aluminum silicate and gypsum. Basically, the mineralogical content of SPV200 is typical of Na-type bentonite, similar to MX-80 bentonite [28,29].



**Figure 1.** Powder X-ray diffractograms of the SPV200 bentonite.

SPV200 bentonite specimens were compacted at an as-received water content of 10.8% in different steel molds for the NP method and TPS method, as shown in Figure 2a,b respectively. Figure 2a shows the compacted specimen consisting of two half-cylinders ( $D = 100$  mm,  $H = 100$  mm) with a vertical hole ( $d = 10$  mm) in the center so that it can be easily assembled with a column ready to be placed by the thermal probe instead of destructively drilling a hole through the height of the specimen as used by other studies [30–34]. Figure 2b is a bentonite disk 100 mm in diameter and 20 mm in height statically compacted inside a steel basin for the transient plane source testing.



**Figure 2.** Specimen preparation for (a) NP method and (b) TPS method.

## 2.2. Experiment Methodology

The apparatus based on the NP method is a PC-based experimental system, as shown in Figure 3, for data collection, monitoring, recording, and analysis of the thermal property of compacted bentonite. The core part is the MX100 DAQ (Yokogawa Devices), which is operated following the specifications in accordance with ASTM 5334-14 [35].

The thermal needle probe shall be calibrated in advance according to ASTM 5334-14 for each continuous measurement. Calibration is especially important because the probe may cause potentially significant differences in estimation of the thermal conductivity due to non-negligible heat storage and transmission in the needle probe itself. Calibration is performed by comparing the thermal conductivity of the material to be measured with

the known value of the calibration material (e.g., water, 0.607 W/m·K). Additionally, the calibration factor is calculated, as shown in Equation (1):

$$C = \frac{\lambda_{material}}{\lambda_{measured}} \quad (1)$$

where  $C$  is the calibration factor,  $\lambda_{material}$  is the known thermal conductivity of the calibration material,  $\lambda_{measured}$  is the thermal conductivity of the material to be measured with the thermal needle probe.

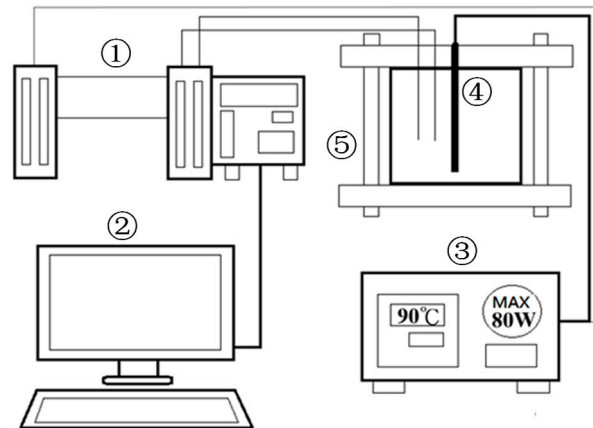


**Figure 3.** PC-based experimental system for the NP method. ① MX100 DAQ, ② computer, ③ heat supplier, ④ thermal needle probe, ⑤ steel frame.

Suitable materials with known thermal conductivity are glycerin with a thermal conductivity of 0.286 W/m·K at 25 °C and water stabilized with 5 g of agar per liter (in prevention of free convection) with a thermal conductivity of 0.607 W/m·K at 25 °C. The latter was used in this study for calibration. The needle probe was coated with thermal grease to minimize contact resistance. To prevent errors coming from free convection, the water specimen was physically stabilized by adding agar into hot water and was stirred well until the mixture was homogenous. The mixture was then brought to a boil and then re-homogenized in the container to be used to hold the specimen during calibration. After cooling down to room temperature, the mixture is a solid with the consistency of jelly, as shown in Figure 4. After calibration, SPV200 specimen was compacted in the mold and inserted with the needle probe through the center hole for measurement, as shown in Figure 5.



**Figure 4.** Calibration for the NP method.



**Figure 5.** Specimen with the thermal probe.

The thermal needle-probe method determines the thermal conductivity of soil using the transient heat method. The set up of the method is considered a close imitation of the heat conduction in a HLW repository with the heat-generating canister being placed in the center of a borehole and surrounded by buffer material. To maintain highly tight contact between the compacted bentonite and the needle-shaped probe, extra care must be exercised to assure good heat conduction at the interface.

Then, the thermal conductivity is determined using Equation (2), which is the slope of a straight line representing the temperature versus  $\ln(t)$  for the transient heating phase.

$$\lambda = \frac{CQ}{4\pi S} \quad (2)$$

and

$$Q = I^2 \frac{R}{L} = \frac{EI}{L} \quad (3)$$

where  $C$  is calibration factor,  $\lambda$  is thermal conductivity ( $\text{W}/\text{m}\cdot\text{K}$ ),  $S$  is the slope used in calculating the thermal conductivity,  $t$  is time (s),  $I$  is the current passing through the heater wire (A),  $R$  is the total resistance of the heater wire ( $\Omega$ ),  $L$  is the length of the heated needle (m), and  $E$  is the measured voltage (V).

As a non-destructive method for measurement of thermal conductivity, the apparatus based on the TPS method is a portable device (ISOMET model 2104, Applied Precision Ltd., Bratislava, Slovakia), as shown in Figure 6, for direct measurement of thermophysical properties of a wide range of materials. These surface probes can be used both as a heat source and a temperature sensor. The probe is placed in good contact with a flat and slightly polished surface of a sample and a transient-heating signal is transmitted. By recording and analyzing the rise or decay of the temperature with time, the thermal properties of the sample, i.e., the thermal conductivity, the thermal diffusivity, the volumetric heat capacity, and the temperature of the sample, can be obtained. Surface probes are more appropriate than needle probes when there are difficulties in drilling for a narrow and long hole with a constant diameter. It applies a dynamic method, which reduces the time for the thermal conductivity measurements to about 10 min. The measurement is based on the analysis of the time dependence of the thermal response of a tested material on the impulses of heat flux, the concept of which is consistent with the TPS method and in compliance with ISO 22007-2:2015 [36].

The operation of the TPS method is straightforward by emplacing the thermal surface probe on the surface of the specimen. With the wait for a steady heat flux of about 10 min, the result is displayed on the screen. However, it is suggested by the manufacturer that testing using the surface probe method is in the temperature range of  $-15\text{ }^\circ\text{C}$  to  $50\text{ }^\circ\text{C}$ .

For both experimental methods, the testing conditions included combinations of the following variables: dry density ranging from  $1.4\text{ g}/\text{cm}^3$  to  $1.7\text{ g}/\text{cm}^3$ , water content from 10.8% to 31.0%, and temperature from  $25\text{ }^\circ\text{C}$  to  $80\text{ }^\circ\text{C}$  (maximum  $50\text{ }^\circ\text{C}$  for ISOMET model

2104). The thermal conductivity was measured at least three times, and the average is used for each specimen.



**Figure 6.** ISOMET-based experimental system for the TPS method.

For the preparation of different specimens with varied dry densities, the bentonite powder with calculated weight was compressed statically into the different steel molds previously shown in Figure 2 to obtain compacted bentonite specimens at the targeted dry density. For the preparation of different specimens with varied water contents, the bentonite powder was firstly wetted by spraying the calculated amount of distilled water to achieve the desired water content. Then, it was carefully mixed and stored in a sealed bag or container at the room temperature of 25 °C for seven days to homogeneously distribute the water [31].

For the measurements of the different specimens with varied temperatures, the compacted specimen, wrapped in plastic and sealed with adhesive tape to prevent a change in moisture, was placed into a small thermotank at the temperatures of 25, 50, 60, 70, and 80 °C, respectively, with the precision of  $\pm 0.1$  °C. It should be noted that for each specimen, about 5 h was needed to reach the temperature equilibrium, while it took at least 72 h to ensure the complete redistribution of water within the specimen [32].

### 3. Experimental Results and Discussion

#### 3.1. Thermal Conductivity of SPV200 Bentonite Based on the NP and TPS Methods

Figure 7 shows the thermal conductivity of compacted SPV200 bentonite determined by the NP and TPS methods with varying dry densities at an as-received bentonite water content of 10.8% and room temperature of 25 °C. The results show that the thermal conductivity of compacted SPV200 bentonite increases with the increase in dry density, and a linear relationship can be observed. This is similar to the findings obtained by other researchers [37,38] from different bentonites. The phenomenon may be explained by the fact that the voids between particles are reduced with the increase of dry density as bentonite is statically compressed with much greater pressure to attain the desired dry density. Moreover, the increase of dry density means increasing the contact area between the particles (bentonite and water particles), leading to a better performance of heat transmission and an increase in its thermal conductivity.

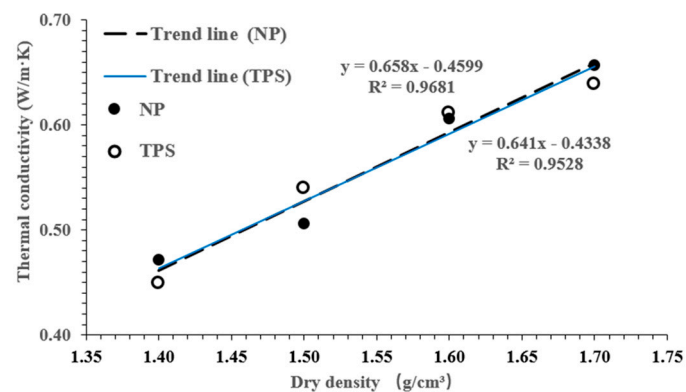


**Figure 7.** Thermal conductivity of compacted bentonite at varying dry densities.

It is also noted that the thermal conductivities measured by the NP method and by the TPS method are very close in Figure 7. For comparison, more measurement results, including the means and standard deviations, obtained by the two methods at different temperatures are presented in Figure 8 (water content of 10.8%). It can be seen from Figure 8, at the 0.05 level of significance, one-way ANOVA indicates that the means derived from the two methods at each dry density are not significantly different. Considering that the NP method is more time-consuming and labor-demanding in the preparation of the compacted specimens, the TPS method is recommended for testing of the thermal conductivity of compacted bentonite at temperatures below 50 °C.

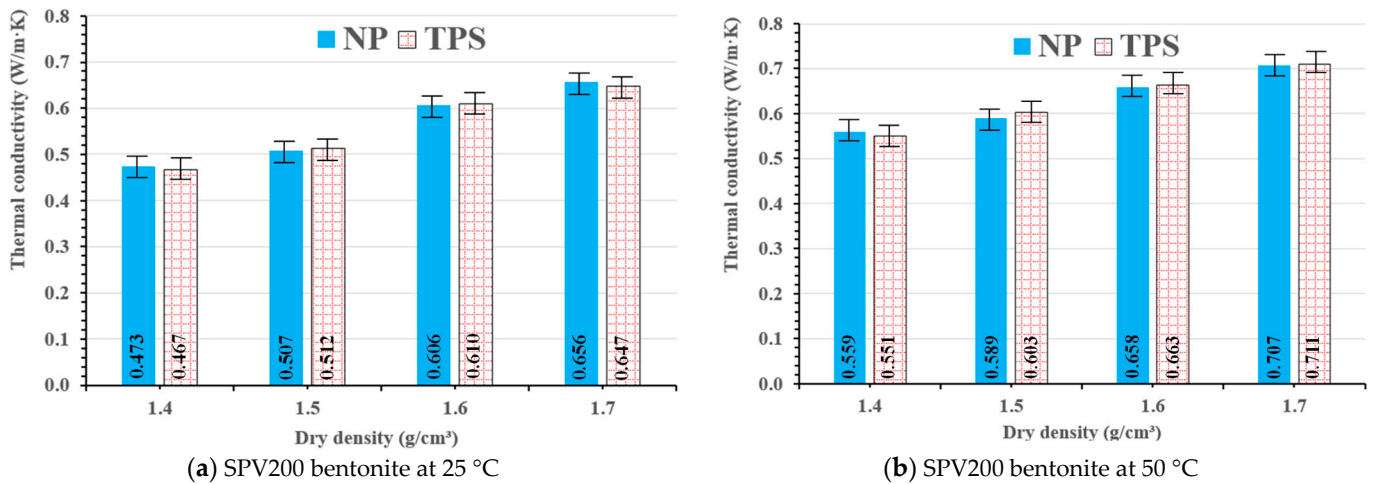


Figure 8. Comparison of thermal conductivities determined using NP and TPS methods.

The thermal conductivity of SPV200 bentonite at constant dry densities with varying water contents was determined by the TPS method at room temperature (25 °C). The dry density of the tested bentonite included 1.7 g/cm<sup>3</sup>, 1.6 g/cm<sup>3</sup>, 1.5 g/cm<sup>3</sup>, and 1.4 g/cm<sup>3</sup>, and the results are shown in Figure 9. All four linear regressions exhibit R-squared values greater than 0.98. The thermal conductivity was observed to increase proportionally to the increase in water content at different densities. The water content is defined as the ratio of the weight of water to the weight of a dry solid. As the water content increases, water with a higher thermal conductivity (0.607 W/m·K) will replace air with a lower thermal conductivity (0.024 W/m·K) in the void of the compacted bentonite. Finally, it leads to an increase of the thermal conductivity of the compacted bentonite.

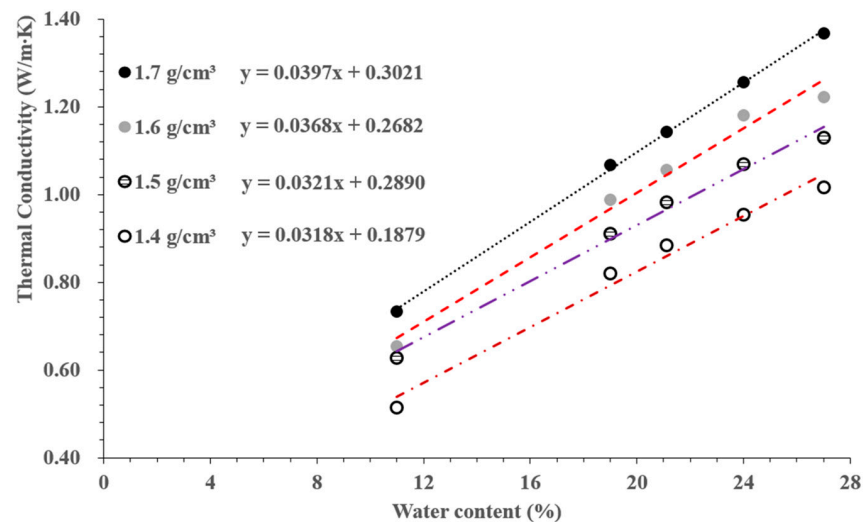
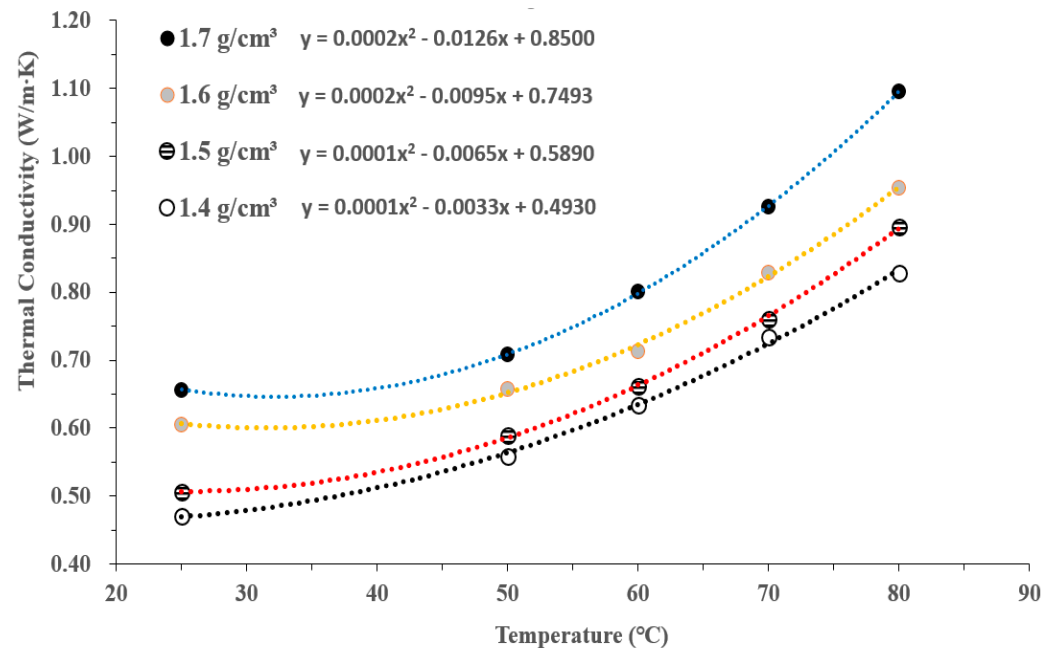


Figure 9. Thermal conductivity of compacted bentonite at varying water contents.

Considering the thermal environment in a repository, measurements were made on compacted bentonites at elevated temperatures using the NP method. The results shown in Figure 10 reveals that for varying dry densities the thermal conductivity of compacted bentonites increases with increasing temperature. All four linear regressions exhibit R-squared values greater than 0.97 in Figure 10. With increasing temperature, the thermal conductivity of water and air increases. Moreover, for the compacted bentonite, it is supposed that its overall thermal conductivity is a combination of the thermal conductivities of the solid phase substance, water, and air. Therefore, the thermal conductivity of compacted bentonites increases with increasing temperature.



**Figure 10.** Thermal conductivity vs. temperatures based on the NP method.

In Figure 10, the thermal conductivity of SPV bentonite increases slowly with temperatures from 20 °C to 50 °C, while the increase becomes noticeable at temperatures greater than 50 °C. For dry densities ranging from 1.4 g/cm<sup>3</sup> to 1.7 g/cm<sup>3</sup>, the change in thermal conductivity with temperature shares a similar trend.

### 3.2. Comparison of Thermal Conductivity of SPV200 Bentonite with Other Bentonites

Figure 11 shows the measured thermal conductivity of many different bentonites having similar mass water content at various dry densities. All the bentonites exhibit increasing thermal conductivity with increases in dry density, and the increasing rate appears to be very close. Meanwhile, it seems that the thermal conductivity of compacted bentonites can be divided into two groups. In the density range of 1.4 g/cm<sup>3</sup> to 1.7 g/cm<sup>3</sup>, the thermal conductivities of SPV 200, MX80, and GMZ bentonites fall in the lower group, ranging from 0.44 W/m·K to 0.70 W/m·K, while that of FEBEX, Kyeongju, and KV1 bentonites are in a somewhat higher group, ranging from 0.61 W/m·K to 0.89 W/m·K.

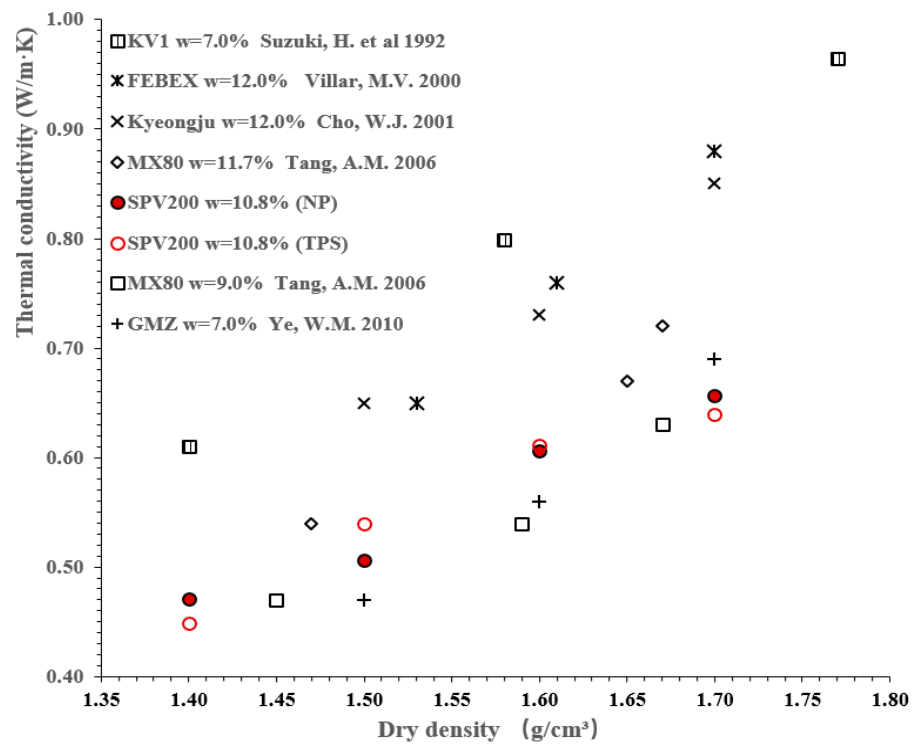


Figure 11. Thermal conductivity vs. dry density relationship for various compacted bentonites [11, 16,38–40].

Figure 12 plots the relationship between measured thermal conductivity and water content of various bentonites compacted to a constant density of 1.6 g/m<sup>3</sup>. It is noticed that the thermal conductivity of bentonite spans over a broader range of 0.4 W/m·K to 1.5 W/m·K for the varying water contents from 5% to 26%. This indicates that the thermal conductivity is more sensitive to the water content than the dry density. Apparently, increased dry density will reduce the porosity and improve the contact conditions between bentonite particles. However, bentonites with higher water content indicates that more voids are filled with water, which is more efficient in heat conduction [30,39–42]. The data in Figure 12 show that the thermal conductivities of most bentonites are very close at varying water content levels, with the KV1 bentonite having slightly higher thermal conductivity than others.

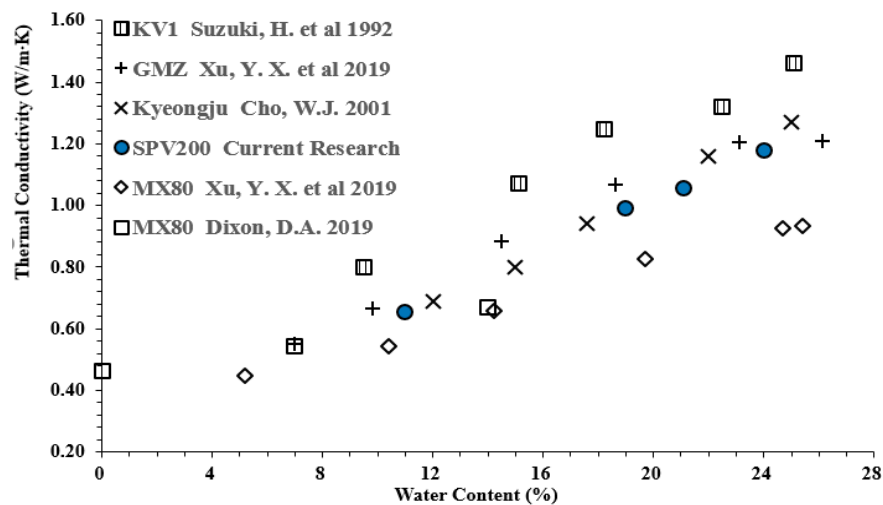


Figure 12. Thermal conductivity vs. water content relationship for various compacted bentonites [10, 32,39,40].

### 3.3. Three-Dimensional Representation of Thermal Conductivity with Water Content and Dry Density

As discussed above, the thermal conductivity of SPV200 bentonite increases approximately linearly with dry density and water content. To illustrate a more explicit relationship among them, Figure 13a generates a 3-D representation of the thermal conductivity of SPV200 bentonite as a function of the dry density and water content. It can be observed that the thermal conductivity increases more rapidly if the water content is raised than the dry density. Figure 13b shows a non-linear surface fit simulated by the software Orginlab, which provides a predicting model with an adjusted R-square of 0.932. The predicting model in Figure 13b can be represented as Equation (4).

$$\lambda = 0.31355 - 0.95859\rho_d + 0.03958\omega + 0.6\rho_d^2 - 6.96848 \times 10^{-5}\omega^2 - 0.00426\omega\rho_d \quad (4)$$

where  $\lambda$  is the thermal conductivity (at room temperature 25 °C),  $\omega$  is the water content (10.8%–31.0%) of compacted SPV200 bentonite, and  $\rho_d$  is the dry density (1.4 g/cm<sup>3</sup>–1.7 g/cm<sup>3</sup>).

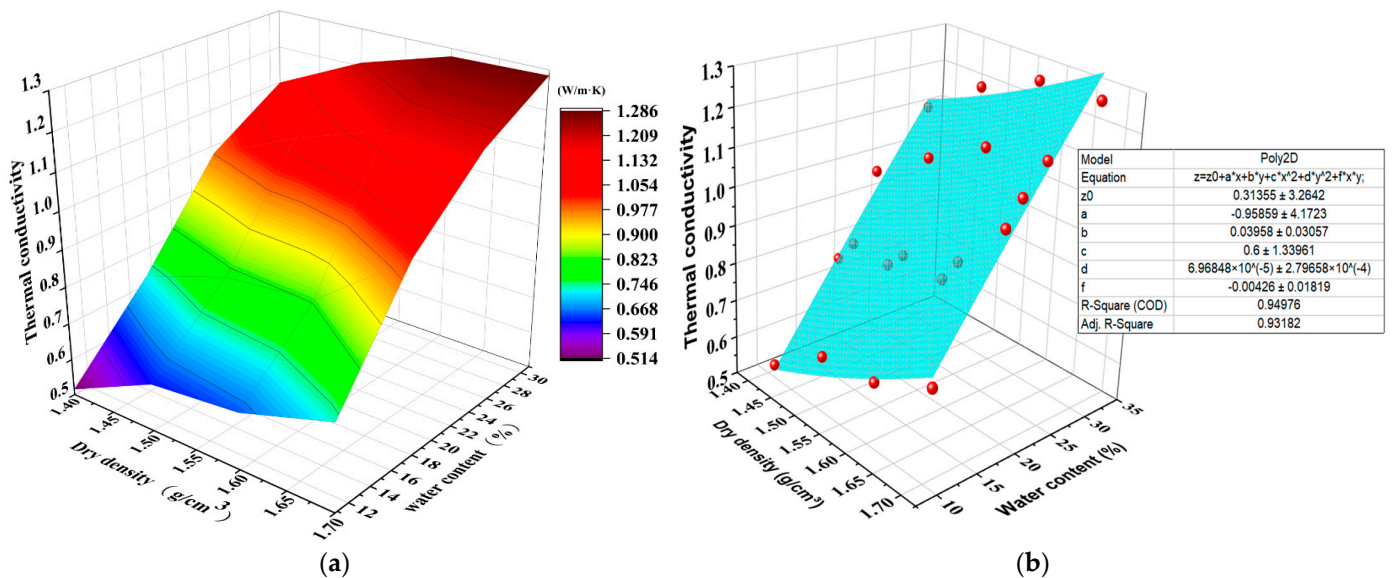


Figure 13. Thermal conductivity ( $\lambda$ -D-W): (a) 3-D representation; (b) 3-D non-linear surface fit.

### 3.4. D Representation of Thermal Conductivity with Dry Density and Temperature

As discussed earlier, the thermal conductivity of SPV200 bentonite increases with dry density and temperature. To give a clear picture of their relationship, Figure 14a generates a 3-D representation of the thermal conductivity of SPV200 bentonite as a function of dry density and temperature ( $\lambda$ -D-T). It is observed that the thermal conductivity of bentonite is very sensitive to changes in temperature. Figure 14b is a non-linear surface fit obtained from the software Orginlab, which provides a predicting model with an adjusted R-square of 0.967. The predicting model in Figure 14b can be represented as Equation (5).

$$\lambda = 2.37198 - 2.77132\rho_d - 0.001032T + 1.07\rho_d^2 - 1.35841 \times 10^{-4}T^2 + 0.00191T\rho_d \quad (5)$$

where  $\lambda$  is the thermal conductivity (at the water content  $\omega = 13\%$ ), T is the temperature (25 °C–80 °C) of compacted SPV200 bentonite, and  $\rho_d$  is the dry density (1.4 g/cm<sup>3</sup>–1.7 g/cm<sup>3</sup>).

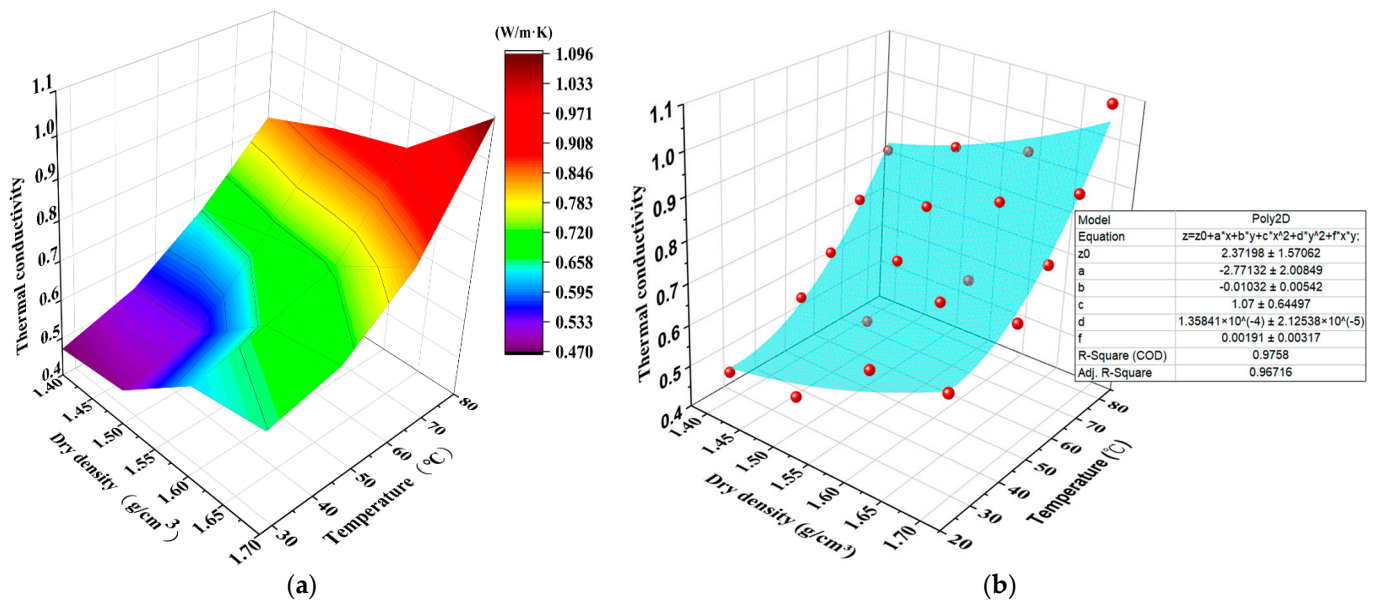


Figure 14. Thermal conductivity ( $\lambda$ -D-T): (a) 3-D representation; (b) 3-D non-linear surface fit.

### 3.5. Comparison between the Calculated and Measured Thermal Conductivity

Since the thermal conductivity of compacted bentonite is highly affected by its water content, temperature, and dry density, a predicting model capable of dealing with the ever-changing conditions of bentonite is of great importance in the simulation of the coupled thermal-hydro-mechanical processes of bentonite. Therefore, 3-D representations in Figures 13 and 14 can provide a quick estimate of the thermal conductivity of bentonite. Figure 15 presents the thermal conductivities calculated using Equations (4) and (5) versus the measured values for compacted SPV200 bentonite. As shown in the figure, all the predicted values fall within the  $\pm 15\%$  relative error bound. The thermal conductivity model with equations can support numerical simulation in the thermal analysis of the bentonite buffer for an HLW repository.

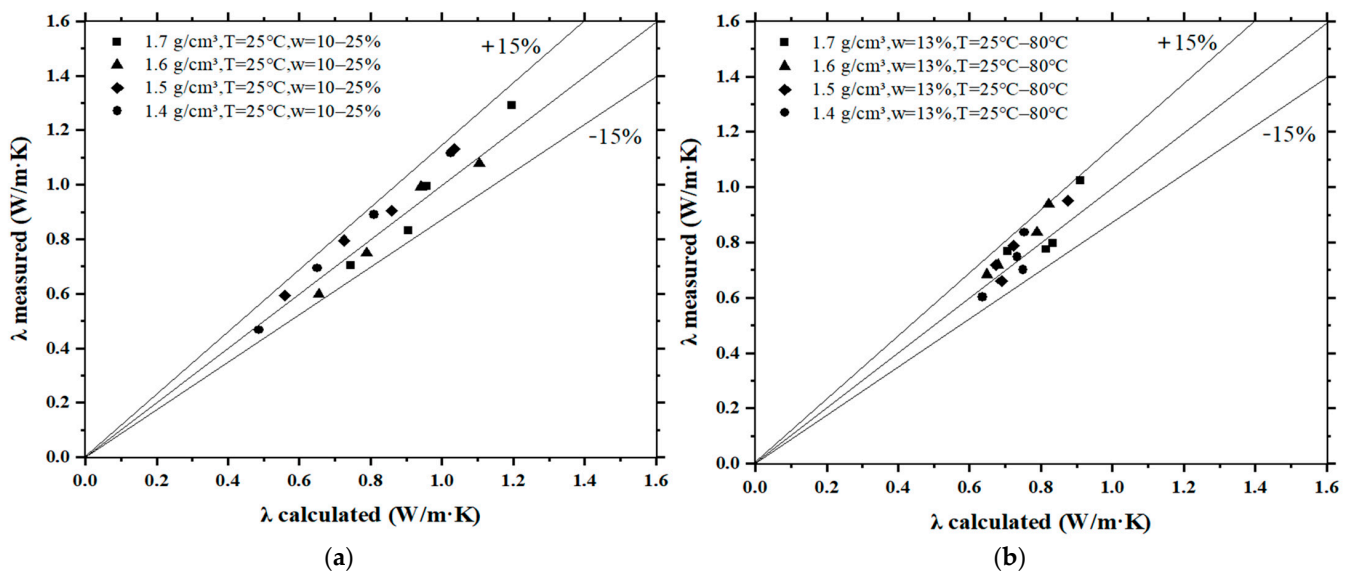


Figure 15. Comparison between the calculated and measured thermal conductivities (a) calculated by Equation (4) vs. measured; (b) calculated by Equation (5) vs. measured.

#### 4. Conclusions

This study measured the thermal conductivity of SPV200 bentonite as a candidate for buffer in the HLW repository and investigated the influence of dry density, water content, and temperature of the compacted bentonite on the thermal conductivity. The experimental methodology demonstrated that the NP method was featured as its simulation for the way of heat conduction in a HLW deposition hole, while the TPS method was highlighted in its practical convenience in measurement. While the measured data from the NP method and TPS method agreed very well, the obtained results showed that the thermal conductivity of compacted SPV200 bentonite was influenced by the dry density, water content, and temperature. Finally, by best fitting the experimental data, this study proposed two predicting models with 3-D visualization for the thermal conductivity of compacted SPV200 bentonite, which may be useful in modelling the coupled T-H-M processes of the bentonite in a HLW repository.

**Author Contributions:** Conceptualization, G.-L.R.; methodology, C.-E.T. and G.-L.R.; investigation and data curation, C.-E.T. and C.-J.C.; writing—original draft preparation, G.-L.R.; writing—review and editing, C.-C.C. and W.-H.H.; funding acquisition, W.-H.H. All authors have read and agreed to the published version of the manuscript.

**Funding:** Partially funded by the Fuel Cycle and Materials Administration, AEC, Taiwan under project number 107FCMA003.

**Institutional Review Board Statement:** Not applicable.

**Informed Consent Statement:** Not applicable.

**Data Availability Statement:** Not applicable.

**Acknowledgments:** We would like to thank the research assistants in the Center of Quality Assurance at National Central University, Taiwan for their kind assistance in performing the experiments.

**Conflicts of Interest:** The authors declare no conflict of interest.

#### References

1. Pusch, R. *The Microstructure of MX-80 Clay with Respect to Its Bulk Physical Properties under Different Environmental Conditions*; Technical Report TR-01-08; SvenskKärnbränslehantering AB (SKB): Stockholm, Sweden, 2001.
2. Pintado, X.; Hassan, M.d.M.; Martikainen, J. *Thermo-Hydro-Mechanical Tests of Buffer Material*; Report 2012-49; POSIVA: Eurajoki, Finland, 2013.
3. Abarca, E.; Sampietro, D.; Sanglas, J.; Molinero, J. *Modelling of the Near-Field Hydrogeology*; Report for the safety assessment SR-PSU.; Technical Report R-19-20; SvenskKärnbränslehantering AB (SKB): Stockholm, Sweden, 2020.
4. Hoek, J.; Hartley, L.; Baxter, S. *Hydrogeological Modelling for the KBS-3H Safety Case*; Report 2016-21; POSIVA: Eurajoki, Finland, 2018.
5. Karvonen, T. *Safety Case for the Operating Licence Application: Surface and Near Surface Hydrological Modelling*; Report 2020-23; POSIVA: Eurajoki, Finland, 2021.
6. Liu, Y.M.; Chen, Z.R. Bentonite from GaoMiaozi, inner mongolia as an ideal buffer/backfilling material in handling highly radioactive wastes—A feasibility study. *Acta Mineral. Sin.* **2001**, *21*, 541–543. [[CrossRef](#)]
7. Alberdi, J.; Barcala, J.M.; Campos, R.; Cuevas, A.M.; Fernandez, E. *FEBEX Project: Full-Scale Engineered Barriers Experiment for a Deep Geological Repository for High Level Radioactive Waste in Crystalline Host Rock Final Report (ENRESA-1/2000)*; Office for Official Publications of the European Communities: Madrid, Spain, 2000.
8. Komine, H. Design flow for specifications of bentonite-based buffer from the viewpoint of self-sealing capability using theoretical equations for swelling characteristics. In Proceedings of the 15th Asian Regional Conference on Soil Mechanics and Geotechnical Engineering, Fukuoka, Japan, 9–13 November 2015; Japanese Geotechnical Society Special Publication: Tokyo, Japan, 2015. [[CrossRef](#)]
9. Madsen, F.T. Clay mineralogical investigations related to nuclear waste disposal. *Clay Miner* **1998**, *33*, 109–129. [[CrossRef](#)]
10. Dixon, D.A. *Review of the T-H-M-C Properties of MX-80 Bentonite*; NWMO-TR-2019-07; NWMO: Toronto, ON, Canada, 2019.
11. Villar, M.V. Caracterización termo-hidro-mecánica de una bentonitade Cabo de Gata. Ph.D. Thesis, Universidad Complutense de Madrid, Madrid, Spain, 2000.
12. Rutqvist, J. Thermal management associated with geologic disposal of large spent nuclear fuel canisters in tunnels with thermally engineered backfill. *Tunn. Undergr. Space Technol.* **2020**, *102*, 4–11. [[CrossRef](#)]

13. Ould-Lahoucine, C.; Sakashita, H.; Kumada, T. Measurement of thermal conductivity of buffer materials and evaluation of existing correlations predicting it. *Nucl. Eng. Des.* **2002**, *216*, 1–11. [[CrossRef](#)]
14. Huang, W.H. Experimental study on the thermo- and hydro-properties of two bentonites as buffer materials. In Proceedings of the EGU General Assembly 2020, Online, 4–8 May 2020. EGU2020-19178. [[CrossRef](#)]
15. Huang, W.H.; Chen, W.C. Swelling behavior of a potential material under simulated near field environment. *J. Nucl. Sci. Technol.* **2004**, *41*, 1271–1279. [[CrossRef](#)]
16. Ye, W.M.; Chen, Y.G.; Chen, B.; Wang, Q.; Wang, J. Advances on the knowledge of the buffer/backfill properties of heavily-compacted GMZ bentonite. *Eng. Geol.* **2010**, *116*, 12–20. [[CrossRef](#)]
17. Xu, Y.; Zhou, X.; Sun, D.; Zeng, Z.T. Thermal properties of GMZ bentonite pellet mixtures subjected to different temperatures for high-level radioactive waste repository. *Acta Geotech.* **2022**, *17*, 981–992. [[CrossRef](#)]
18. Cho, W.J.; Lee, J.O.; Kwon, S.K. Thermal Conductivity of Compacted Bentonite and Bentonite-Sand Mixture. *J. Nucl. Fuel Cycle Waste Technol.* **2008**, *6*, 101–109.
19. Yoon, S.; Jeon, J.S.; Kim, G.Y.; Seong, J.H.; Baik, M.H. Specific heat capacity model for compacted bentonite buffer materials. *Ann. Nucl. Energy* **2019**, *125*, 18–25. [[CrossRef](#)]
20. DeVries, D.A. Thermal Properties of Soils. In *Physics of Plant Environment*; van Wijk, W.R., Ed.; North-Holland Publishing Co.: Amsterdam, The Netherlands, 1963; pp. 210–235.
21. Nikolaev, I.V.; Leong, W.H.; Rosen, M.A. Experimental investigation of soil thermal conductivity over a wide temperature range. *Int. J. Thermophys.* **2013**, *34*, 1110–1129. [[CrossRef](#)]
22. Johansen, O. Thermal conductivity of soils. Ph.D. Dissertation, Norwegian University of Science and Technology, Trondheim, Norway, 1975.
23. Cho, W.J.; Lee, J.O.; Kwon, S. An empirical model for the thermal conductivity of compacted bentonite and a bentonite-sand mixture. *Heat Mass Transf.* **2011**, *47*, 1385–1393. [[CrossRef](#)]
24. Chen, Y.G.; Liu, X.M.; Mu, X.; Ye, W.M.; Cui, Y.J.; Chen, B.; Wu, D.B. Thermal Conductivity of Compacted GO-GMZ Bentonite Used as Buffer Material for a High-Level Radioactive Waste Repository. *Adv. Civil. Eng.* **2018**, *4*, 1–11. [[CrossRef](#)]
25. Bang, H.T.; Yoon, S.; Jeon, H. Application of machine learning methods to predict a thermal conductivity model for compacted bentonite. *Ann. Nucl. Energy.* **2020**, *142*, 1–11. [[CrossRef](#)]
26. Kim, M.J.; Lee, G.J.; Yoon, S. Numerical Study on the Effect of Enhanced Buffer Materials in a High-Level Radioactive Waste Repository. *Appl. Sci.* **2021**, *11*, 8733. [[CrossRef](#)]
27. Vieira, A.; Alberdi-Pagola, M.; Christodoulides, P.; Javed, S.; Loveridge, F.; Nguyen, F.; Cecinato, F.; Maranha, J.; Florides, G.; Prodan, I.; et al. Characterisation of Ground Thermal and Thermo-Mechanical Behaviour for Shallow Geothermal Energy Applications. *Energies* **2017**, *10*, 2044. [[CrossRef](#)]
28. Kumar, R.S.; Podlech, C.; Grathoff, G.; Warr, L.N.; Svensson, D. Thermally Induced, Bentonite Alterations in the SKB ABM5 Hot Bentonite Experiment. *Minerals* **2021**, *11*, 1017. [[CrossRef](#)]
29. Holmboe, M.; Wold, S.; Jonsson, M. Porosity investigation of compacted bentonite using XRD profile modeling. *J. Contam. Hydrol.* **2012**, *128*, 19–32. [[CrossRef](#)]
30. Sakashita, H.; Kumada, T. Heat transfer model for predicting thermal conductivity of highly compacted bentonite. *J. Jpn. At. Soc.* **1998**, *40*, 235–240.
31. Tang, A.M.; Cui, Y.J.; Le, T.T. A study on the thermal conductivity of compacted bentonites. *Appl. Clay Sci.* **2008**, *41*, 181–189. [[CrossRef](#)]
32. Xu, Y.S.; Zeng, Z.T.; Lv, H.B. Temperature dependence of apparent thermal conductivity of compacted bentonites as buffer material for high-level radioactive waste repository. *Appl. Clay Sci.* **2019**, *174*, 10–14. [[CrossRef](#)]
33. Ortiz de Zárate, J.M.; Hita, J.L.; Khayet, M.; Legido, J.L. Measurement of the thermal conductivity of clays used in pelotherapy by the multi-current hot-wire technique. *Appl. Clay Sci.* **2010**, *50*, 423–426. [[CrossRef](#)]
34. Alrtimi, A.; Rouainia, M.; Manning, D.A.C. An improved steady-state apparatus for measuring thermal conductivity of soils. *Int. J. Heat Mass Transf.* **2014**, *72*, 630–636. [[CrossRef](#)]
35. ASTM D 5334-14; Standard Test Method for Determination of Thermal Conductivity of Soil and Soft Rock by Thermal Needle Probe Procedure. ASTM, 100 Barr Harbor Dr.: West Conshocken, PA, USA, 2014. Available online: <https://www.en-standard.eu/d5334-14-standard-test-method-for-determination-of-thermal-conductivity-of-soil-and-soft-rock-by-thermal-needle-probe-procedure/> (accessed on 25 June 2022).
36. ISO 22007-2; Determination of Thermal Conductivity and Thermal Diffusivity—Part 2: Transient Plane Heat Source (Hot Disc) Method. ISO Copyright Office: Geneva, Switzerland, 2015.
37. Gustafsson, S.E. Transient plane source techniques for thermal conductivity and thermal diffusivity measurements of solid materials. *Rev. Sci. Instrum.* **1991**, *62*, 797–798. [[CrossRef](#)]
38. Tang, A.M.; Cui, Y. Determining the Thermal Conductivity of Compacted MX80 Clay. Geotechnical Special Publication. In Proceedings of the Fourth International Conference on Unsaturated Soils, Carefree, AZ, USA, 2 April 2006; pp. 1695–1706. [[CrossRef](#)]
39. Cho, W.J.; Lee, J.W.; Kang, C.H. A Compilation and Evaluation of Thermal and Mechanical Properties of Compacted Bentonite for the Performance Assessment of Engineered Barriers in the High-Level Waste Repository; KAERI Report, KAERI/TR–1826/2001. KR0100897; Korea Atomic Energy Research Institute, Taejeon: Daejeon, Korea, 2001. (In Korean)

40. Shen, Z.Y.; Li, G.D.; Li, S.K. Thermal property of highly compacted bentonite, Embankment. *Obs. Soil Test.* **2001**, *22*, 39–40. (In Chinese)
41. Lee, J.O.; Choi, H.; Lee, J.Y. Thermal conductivity of compacted bentonite as a buffer material for a high-level radioactive waste repository. *Ann. Nucl. Energy* **2016**, *94*, 848–855. [[CrossRef](#)]
42. Suzuki, H.; Shibata, M.; Yamagata, J.; Hirose, I.; Terakado, K. Physical and Mechanical Properties of Bentonite (I). *PNC TN1410* **1992**, 92-052. (In Japanese)